The electron density in flavones I. Baicalein†

David. E. Hibbs,[a] Jacob Overgaard,[a] Carlo Gatti[b] and Trevor W. Hambley[a]

[a] *School of Chemistry, University of Sydney, Sydney NSW 2006, Australia. E-mail: d.hibbs@chem.usyd.edu.au; Fax: +61 (0)2 9351 3329; Tel: +61 (0)2 9036 9122*
[b] *Istituto di Scienze e Tecnologie Molecolari, via Golgi 19, I-20133, Milano, Italy. E-mail: c.gatti@istm.cnr.it; Fax: +39 (0)2 503-14300; Tel: +39 (0)2 503-14277*

Received (in Montpellier, France) 14th February 2003, Accepted 21st March 2003
First published as an Advance Article on the web 9th July 2003

The experimental charge density distribution of 5,6,7-trihydroxyflavone (**1**), has been determined from high-resolution X-ray diffraction data collected at 100 K. Additionally, high level single-point gas-phase calculations as well as periodic calculations have been carried out for (**1**). To our surprise, the topological analysis of the experimental electron density revealed a cage critical point in the geometric center of the tri-hydroxy substituted aromatic ring. This feature was independently confirmed by analysis of another study of **1**. However, both high-level gas-phase and periodic *ab initio* calculations failed to reproduce this feature. The degree of bias on the electron density by using the Hansen–Coppens multipole model was tested by a multipole refinement of generated theoretical structure factors. This clearly showed that the cage critical point is not an artefact resulting from the use of the multipole model. Compound **1** contains a large number of weak, intermolecular hydrogen bonds and these are analysed using the Atoms in Molecules (AIM) approach, which leads to quantitative measures for hydrogen bond strength. The experimentally derived lattice energy of -467 kJ mol^{-1} shows a rather strongly held crystal lattice.

Introduction

Baicalein (5,6,7-trihydroxyflavone) (Fig. 1) is a plant flavonoid, formed *in vivo* by the metabolism of baicalin by the cleavage of the glycoside moiety.[1] The action of baicalein in the body includes inhibition of HIV-1 infection,[2] as well as antioxidant,[3] antifungal, antibacterial, and anti-inflammatory properties.[4] Baicalein is also known to inhibit lipoxygenases.[5] Baicalein has been isolated from *Scutellaria baicalensis*, and has been found to exhibit the enzyme α-glucosidase, thus preventing the absorption of dietary carbohydrates, consequently suppressing postprandial hyperglycemia.[6]

Baicalein and baicalin have both been found to interact with the $GABA_A$ receptor at the benzodiazepine-binding site, with an activity of seven times less than 6-hydroxyflavone at the receptor complex.[7] Our interest in the flavone family is to understand the electronic differences between these structurally similar molecules that differentiate their reactivity. We also aim at building a library of electron density derived molecular properties that eventually will increase the probability of successful output from quantitative structure–activity relationship (QSAR) studies. Furthermore, the baicalein molecule is interesting in itself due to the large range of intermolecular interactions present in the crystal lattice. Therefore, this work will detail the analysis of experimental and theoretical charge density studies of baicalein.

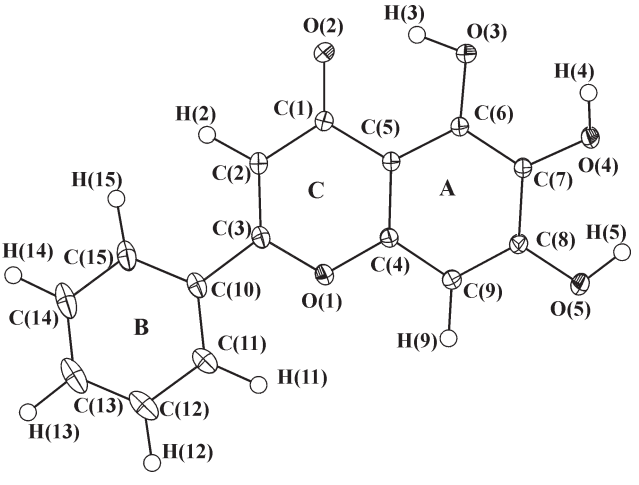

Fig. 1 Thermal ellipsoids drawing of **1** showing 50% probability surfaces.

Experimental section

Molecular orbital calculations

All gas phase DFT calculations were performed with the GAUSSIAN98 program package[8] at the 6-311++G** level of theory, using the three parameter hybrid exchange functional of Becke in combination with the gradient corrected exchange-correlation potential of Lee, Yang and Parr (B3LYP).[9] The AIMPAC suite of programs was used for the topological analysis of the theoretical wavefunctions.[10] All gas-phase calculations were done using the experimental geometry and performed on a Silicon Graphics ORIGIN2400 computer [reference: http://www.ac3.com.au/sgi-origin-2400.htm]. The periodic Hartree Fock and DFT(B3LYP) calculations were carried out using the CRYSTAL98 package,[11] and the results analysed with the program TOPOND98.[12] Due to the size of the system, 120 atoms per cell, the simple double-zeta plus polarization 3-21G(d,p) basis set was

† Electronic supplementary information (ESI) available: refined multipole values, radial parameters used in XD-refinements and topological analysis of O–H and C–H bonds in **1**. See http://www.rsc.org/suppdata/nj/b3/b301740k/

 DOI: 10.1039/b301740k

adopted, with the scale factor of the outermost shell of each atom fixed at 1.2.

X-ray data collection

Crystals of **1** were grown from ethyl acetate by slow evaporation. Single-crystal, high-resolution, low-temperature X-ray diffraction data were collected on a Bruker SMART 1000 CCD based diffractometer. Cell constants were obtained from the least squares refinement of 7393 reflections located between 4.7 and 63.3° 2θ. Three reciprocal space data shells were collected, with one shell providing data between 2 and 58° 2θ, a second for data between 42 and 98° 2θ and a third for data between 72 and 128° 2θ. Data were collected at 100(2) K with ω-scan increments of 0.3°.

The data collection resulted in a total of 65 593 reflections, which were integrated and corrected for Lorentz and polarisation effects using the program SAINT+.[13] The set of intensities were averaged, merged and corrected for absorption using SORTAV.[14] This gave 18 451 unique reflections with a maximum $\sin(\theta)/\lambda$ of 1.25 Å^{-1} and an average redundancy of 3.6.

Structure solution and multipole refinement

The crystal structure was solved with direct methods using SHELXS[15] from all intensities with $I(\boldsymbol{h}) > 2\sigma(I(\boldsymbol{h}))$. All hydrogen bonds were located from difference Fourier maps and refined using the program SHELXL97[15] with isotropic thermal parameters constrained to values 20% higher than the equivalent thermal motion of the parent atom. The X–H bond distances were constrained to average values obtained from neutron diffraction experiments.[16] The set of atomic and thermal parameters were then imported into the electron density least-squares refinement package XD.[17] This program employs the Hansen–Coppens pseudo-atom formalism[18] to describe the molecular electron density. Neutral atomic scattering factors were used for O and C.

In the absence of neutron diffraction data, a high-order refinement ($\sin\theta/\lambda > 0.8$ Å^{-1}) of the atomic and thermal parameters is one way of ensuring a correct deconvolution of the atomic thermal motion from the electron density.[19] This was performed and the resulting structural parameters formed the basis of the multipole refinement. The rigid-bond test of Hirshfeld[20] showed a maximum difference of Δ_{A-B} of 7×10^{-4} Å^2 (C(11)–C(12)) and an average value of 2.4×10^{-4} Å^2, well below the proposed threshold value of 10^{-3} Å^2. On this basis we conclude that the thermal motion has been correctly separated from the electron density distribution, giving enhanced confidence in our model.

The level of multipole expansion was initially truncated at the octopole level ($l_{max} = 3$) for all heavy atoms. In an attempt to improve the model, hexadecapoles ($l_{max} = 4$) were included in the description of the oxygen atoms but only a few of these parameters were populated at a 2σ-level. However, the chemical model that resulted was unrealistically biased by the introduction of the hexadecapolar functions, hence these were omitted in subsequent refinements. With the structural and multipolar parameters fixed, the radial dependency of the aspherical functions (κ'') for each atom type were refined, before a final comprehensive refinement of both structural and multipole parameters. In all refinements, the hydrogens attached to C and O were treated as chemically independent. For each of these two groups of hydrogen atoms, one monopole was refined and the asphericity was described by a single bond-directed dipole. Furthermore, H(3) and H(4) are involved in short hydrogen bonds and for these atoms an additional bond-directed quadrupole ($l_{max} = 2$) was required.

The multipole refinement on F^2 converged with $R(F) = 0.043$. A residual map is shown in Fig. 2. Additional crystallographic details are summarised in Table 1.

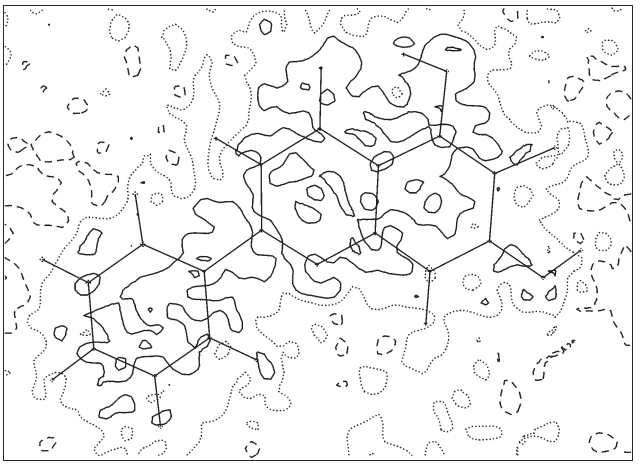

Fig. 2 Residual density in the plane of the molecule. Solid lines show positive contours and dashed lines show negative lines. Contours at ± 0.10 eÅ^{-3}.

Multipole refinement of theoretical structure factors

Based on the periodic DFT(B3LYP) calculation, theoretical structure factors were calculated using the CRYSTAL98 package.[11] To simulate the refinements of experimental structure factors in the best possible way, only those structure factors included in the experimental refinement were generated from the theoretical wavefunction. The thermal parameters were reset to zero and the structural parameters were fixed on the values used for the calculations. The multipoles used were identical to those implemented in the refinement of experimental structure factors, see previous paragraph. For each non-hydrogen atom type, separate κ'' parameters were refined for each value of l. The refinement residual was $R(F) = 0.017$. All refinements were carried out on F using the program XD.[17]

Table 1 Crystallographic details

Empirical formula	$C_{15}H_{10}O_5$
Formula weight/g mol^{-1}	270.23
Crystal system	Monoclinic
Space group	$P2_1/c$
Z	4
Temperature (K)	100(2)
a (Å)	7.7707(5)
b (Å)	13.2373(Å)
c (Å)	11.5427(Å)
β (°)	101.027
V (Å^3)	1167.2
ρ_{calc} (g cm^{-3})	1.196
$F(000)$	440
μ (mm^{-1})	0.12
Crystal size (mm)	$0.30 \times 0.25 \times 0.20$
λ (Å)	0.7107
$\sin(\theta)/\lambda_{max}$(Å^{-1})	1.252
Limiting indices (h; k; l)	$-19 \rightarrow 19$; $0 \rightarrow 32$; $0 \rightarrow 28$
Number of collected reflections	65 593
Symmetry independent reflections	18 451
Average multiplicity	3.6
Reflections with $I > 3\sigma(I)$	8469
Completeness (%)	96.1
R_{int}	0.023
$R(F)$	0.043
$R_w(F^2)$	0.060
S	2.19
Number of variables	420
N_{ref}/N_{var}	20.3

Results and discussion

Crystal structure

The structural details of **(1)** are given in Table 2, with the molecular geometry shown in Fig. 1. The dihedral angle between the phenyl ring and the γ-pyrone ring is *ca* 9.0°, a value small enough to decrease the C(3)–C(10) bond length to 1.4691(7) Å. The overall geometry of **1** is similar to that of other flavones.[21] The existence of this small dihedral angle increases the degree of delocalisation of the π-electrons across the C(3)–C(10) bond, resulting in a partial double-bond character in this bond as well as in the C(1)–C(2) bond. The effect is the aforementioned shortening of the C(3)–C(10) bond compared to the expected bond length of 1.51 Å for a pure single bond. At the same time, the C(2)–C(3) bond length is slightly increased and hence has less than complete double bond character. The C(1)–O(2) bond length is also increased compared to flavones having a larger dihedral angle.[21]

The crystal structure of baicalein exhibits a significant number of inter- and intramolecular C–H···O and O–H···O hydrogen bonds (HBs). These are listed in Table 3, sorted in ascending H···O HB distance. The geometries of the two shortest HBs are almost completely identical, both characterised as relatively strong HBs. It is noteworthy that the intramolecular C–H···O HB, due to a very acute geometry, has a rather short donor-to-acceptor distance. However, the angular geometry of this bond means it is unlikely to be of significant strength. Apart from the non-coplanarity of the phenyl ring and the γ-pyrone ring due to the non-zero dihedral angle, only H(4) is significantly out of the molecular plane. It is 0.49 Å above the γ-pyrone ring, and is involved in the second relatively short HB. Both the relative and absolute strengths of the HBs will be described in relation to the topological analysis in a following section.

Table 2 Final experimental geometry (from XD) of **1** in Å and °

	Distance (Å)		Angle (°)
O(1)–C(3)	1.3532(7)	C(3)–O(1)–C(4)	119.88(5)
O(1)–C(4)	1.3695(7)	O(2)–C(1)–C(2)	122.76(5)
O(2)–C(1)	1.2604(8)	O(2)–C(1)–C(5)	121.17(5)
O(3)–C(6)	1.3478(7)	C(2)–C(1)–C(5)	116.07(5)
O(4)–C(7)	1.3618(7)	C(1)–C(2)–C(3)	121.05(5)
O(5)–C(8)	1.3498(7)	O(1)–C(3)–C(2)	122.19(5)
C(1)–C(2)	1.4316(7)	O(1)–C(3)–C(10)	112.73(5)
C(1)–C(5)	1.4387(7)	C(2)–C(3)–C(10)	125.07(5)
C(2)–C(3)	1.3602(7)	O(1)–C(4)–C(5)	121.17(5)
C(3)–C(10)	1.4691(7)	O(1)–C(4)–C(9)	116.56(5)
C(4)–C(5)	1.4001(7)	C(5)–C(4)–C(9)	122.26(5)
C(4)–C(9)	1.3871(7)	C(1)–C(5)–C(4)	119.61(5)
C(5)–C(6)	1.4143(6)	C(1)–C(5)–C(6)	121.79(5)
C(6)–C(7)	1.3843(7)	C(4)–C(5)–C(6)	118.58(5)
C(7)–C(8)	1.4039(7)	O(3)–C(6)–C(5)	122.13(5)
C(8)–C(9)	1.3925(7)	O(3)–C(6)–C(7)	117.93(5)
C(10)–C(11)	1.3987(8)	C(5)–C(6)–C(7)	119.92(5)
C(10)–C(15)	1.4024(8)	O(4)–C(7)–C(6)	122.56(5)
C(11)–C(12)	1.3920(8)	O(4)–C(7)–C(8)	117.76(5)
C(12)–C(13)	1.3926(14)	C(6)–C(7)–C(8)	119.67(4)
C(13)–C(14)	1.3927(14)	O(5)–C(8)–C(7)	120.07(5)
C(14)–C(15)	1.3860(9)	O(5)–C(8)–C(9)	118.39(5)
		C(7)–C(8)–C(9)	121.55(4)
		C(4)–C(9)–C(8)	117.84(4)
		C(3)–C(10)–C(11)	120.58(6)
		C(3)–C(10)–C(15)	120.27(6)
		C(11)–C(10)–C(15)	119.14(6)
		C(10)–C(11)–C(12)	120.08(7)
		C(11)–C(12)–C(13)	120.47(7)
		C(12)–C(13)–C(14)	119.53(6)
		C(13)–C(14)–C(15)	120.36(8)
		C(10)–C(15)–C(14)	120.39(7)

Table 3 Experimental hydrogen bond lengths (Å) and angles (°)of **1**

D–H···A	*d*(D–H)	*d*(D···A)	*d*(H···A)	∠(D–H···A)
O(4)–H(4)···O(2)[a]	0.970	2.616(1)	1.71	153.4
O(3)–H(3)···O(2)	0.970	2.611(1)	1.74	148.2
O(5)–H(5)···O(4)[b]	0.970	2.787(1)	1.95	142.7
C(11)–H(11)···O(1)	1.083	2.711(1)	2.38	95.9
C(9)–H(9)···O(3)[c]	1.083	3.395(1)	2.88	109.6
C(14)–H(14)···O(5)[d]	1.083	3.331(1)	2.95	101.2
C(14)–H(14)···O(4)[d]	1.083	3.726(1)	3.06	120.3
C(12)–H(12)···O(2)[e]	1.083	3.590(1)	3.16	104.5
C(11)–H(11)···O(5)[f]	1.083	3.837(1)	3.30	112.0
C(13)–H(13)···O(2)[g]	1.083	4.258(1)	3.30	147.8

[a] $+x, 3/2-y, 1/2+z$ [b] $1-x, 2-y, 2-z$ [c] $1-x, 1/2+y, 3/2-z$ [d] $x, y, -1+z$ [e] $2-x, 2-y, 1-z$ [f] $x, 5/2-y, -1/2+z$ [g] $2-x, 1/2+y, 1/2-z$.

The experimental static deformation density in the plane of the γ-pyrone ring of baicalein is shown in Fig. 3. First of all, it outlines the bonding density in the covalent bonds in (**1**). More interestingly, the deformation density provides a qualitative view of the lone pair structure around the oxygen atoms. For the carboxyl oxygen (O(2)), two slightly distorted lone pairs are apparent in the molecular plane. One of the lone pairs is displaced towards H(3), which bridges in the relatively short intramolecular HB between O(3) and O(2). There are also indications of lone pairs on the other four oxygens in Fig. 3, however the height of the peaks indicates that the selected plane does not intersect the maximum values. Indeed, for O(1) the static deformation density in a plane perpendicular to the molecular plane and containing the O(1)–C(1) line shows two maxima on either side of the plane (Fig. 4). The existence of two lone pairs on O(1) suggests that this ether-oxygen adopts an sp^3-configuration.

A problematic feature of the static deformation density mapping is that it is dependent on the (arbitrary) choice of a suitable reference state to be subtracted from the observed density. Therefore, this method has partly been replaced by

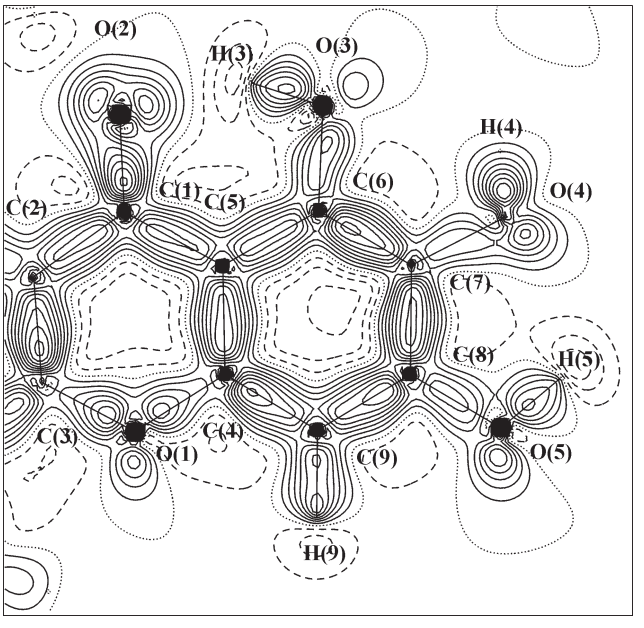

Fig. 3 Static deformation density in the plane of the γ-pyrone ring. Solid lines show positive contours and dashed lines show negative lines. Contours at ± 0.10 eÅ^{-3}.

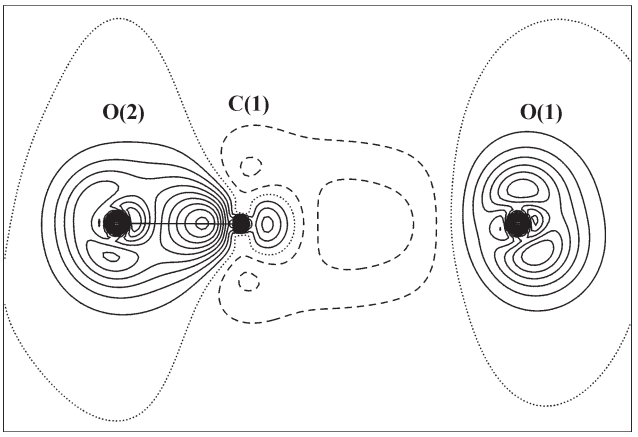

Fig. 4 Static deformation density in a plane perpendicular to the molecular plane including the C(1)–O(1) vector. Contours as in Fig. 3.

the mapping of the negative Laplacian of the electron density, $L(r)$, which is mapped in Fig. 5.

Fig. 5 highlights an often encountered feature in experimental charge density studies, that is the observation of polar and partly not-shared interactions in C–O bonds. This results from a depletion of charge in the interatomic regions due to the increased polarity of the C–O bonds compared to homoatomic bonds. The appearence of the C–O bonds in Fig. 5 confirm the intermediate character of C–O interactions as shown by Bader.[10] The theory of Atoms in Molecules does lead to a classification of these bonds as open-shell, covalent interactions (see next section). It should be noted that such observations are often seen in the literature without being given much mentioning.[22]

Topological analysis of covalent bonds

The negative values of $\nabla^2\rho_{BCP}$ observed for all bonds leads to the classification of all bonds being covalent. However, in order to examine the bonding interactions in more detail, a topological analysis of the electron density using the theory of Atoms in Molecules[10] has been carried out for (**1**) both for the gas-phase single-point theoretical wavefunction and the experimental charge density (Table 4).

It is worthwhile to highlight the differences between experimental and theoretical topologies from Table 4. Significantly higher experimental than corresponding theoretical values for ρ_{BCP} are observed in all C–C and C–O bonds, while the opposite is the case for O–H and C–H (see Supplementary Information†) bonds. However, only the C–O bonds and the bonds involving hydrogens also exhibit highly significant discrepancies in the values of $\nabla^2\rho_{BCP}$, with calculated values in the C–O bonds being highly underestimated compared to experiment. Furthermore, Table 4 also shows a discrepancy in the position of the BCP, most pronounced in the C–O bonds, and less so in the C–C bonds. Calculation predicts the BCP in the C–O bonds to be on average 0.07 Å closer to the carbon than is found experimentally. The corresponding values in the C–C bonds average at 0.01 Å, mainly due to larger differences in the C–C bonds in the phenyl ring.[23] While the electron density is a relatively slowly changing function, the

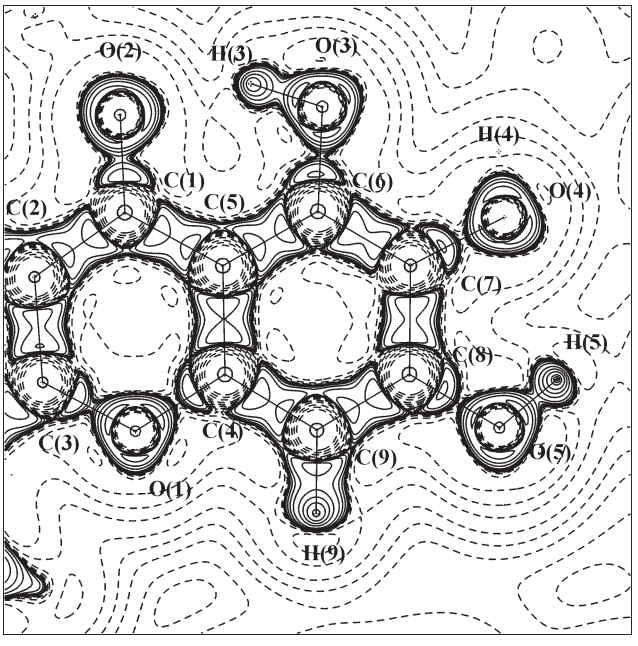

Fig. 5 Negative experimental Laplacian, $L(r)$, of the electron density in the same section as Fig. 3. The solid lines show positive contours, and the dashed lines show negative contours. The contours are shown at intervals of $\pm$ 2, 4, 8×10^n eÅ^{-5}, $n = -3, -2, -1, 0, 1, 2$.

Table 4 Topological analysis of the covalent bonds in **1**. First line gives experimental values, second line gives results from topological analysis of the gas-phase single-point calculation

Bond	ρ_{BCP}/ eÅ^{-3}	$\nabla^2\rho_{BCP}$/ eÅ^{-5}	ε	d_{1-2}/ Å	d_{1-BCP}/ Å	d_{2-BCP}/ Å
O(1)–C(3)	2.11(2)	−16.9(1)	0.18	1.353	0.849	0.505
	1.92	−4.6	0.02	1.353	0.899	0.454
O(1)–C(4)	2.03(2)	−13.9(1)	0.22	1.370	0.837	0.533
	1.84	−4.6	0.00	1.369	0.910	0.460
O(2)–C(1)	2.93(2)	−32.7(1)	0.28	1.260	0.759	0.502
	2.50	−10.1	0.03	1.260	0.827	0.433
O(3)–C(6)	2.25(2)	−17.4(1)	0.20	1.348	0.811	0.537
	2.03	−10.8	0.03	1.348	0.885	0.463
O(4)–C(7)	2.16(2)	−16.1(1)	0.17	1.362	0.808	0.554
	1.91	−7.3	0.07	1.361	0.899	0.462
O(5)–C(8)	2.23(2)	−17.4(1)	0.11	1.350	0.804	0.546
	1.99	−8.8	0.01	1.349	0.891	0.459
C(1)–C(2)	2.04(2)	−17.08(4)	0.27	1.432	0.726	0.706
	1.98	−19.45	0.15	1.432	0.723	0.709
C(1)–C(5)	2.01(1)	−17.03(3)	0.26	1.439	0.729	0.710
	1.96	−18.89	0.15	1.438	0.719	0.719
C(2)–C(3)	2.39(2)	−22.75(5)	0.39	1.360	0.632	0.728
	2.21	−22.79	0.32	1.360	0.632	0.728
C(3)–C(10)	1.89(2)	−15.13(4)	0.26	1.469	0.765	0.704
	1.85	−17.22	0.13	1.469	0.764	0.705
C(4)–C(5)	2.23(2)	−20.05(4)	0.29	1.400	0.714	0.686
	2.07	−20.37	0.25	1.400	0.730	0.670
C(4)–C(9)	2.21(2)	−18.33(4)	0.31	1.387	0.729	0.658
	2.12	−21.32	0.28	1.387	0.731	0.656
C(5)–C(6)	2.08(2)	−16.83(4)	0.30	1.414	0.709	0.706
	2.01	−19.35	0.23	1.414	0.687	0.727
C(6)–C(7)	2.29(2)	−22.41(4)	0.38	1.385	0.716	0.669
	2.16	−22.17	0.34	1.385	0.695	0.690
C(7)–C(8)	2.29(2)	−21.69(4)	0.38	1.404	0.699	0.705
	2.09	−20.82	0.30	1.404	0.694	0.710
C(8)–C(9)	2.20(2)	−18.62(4)	0.30	1.393	0.721	0.672
	2.09	−20.94	0.27	1.393	0.730	0.663
C(10)–C(11)	2.23(2)	−19.56(4)	0.23	1.399	0.707	0.692
	2.06	−20.36	0.20	1.399	0.710	0.689
C(10)–C(15)	2.18(2)	−19.68(4)	0.20	1.403	0.722	0.681
	2.05	−20.11	0.19	1.403	0.708	0.694
C(11)–C(12)	2.17(2)	−18.30(5)	0.11	1.392	0.737	0.655
	2.10	−21.02	0.20	1.392	0.700	0.692
C(12)–C(13)	2.20(2)	−18.34(5)	0.20	1.393	0.660	0.733
	2.09	−21.00	0.19	1.393	0.697	0.696
C(13)–C(14)	2.28(3)	−20.99(6)	0.18	1.393	0.658	0.735
	2.09	−20.97	0.19	1.394	0.698	0.696
C(14)–C(15)	2.25(2)	−20.83(5)	0.19	1.386	0.676	0.711
	2.12	−21.48	0.21	1.386	0.690	0.697

Laplacian function changes rapidly in the interatomic region. Thus, it may be appropriate to evaluate the theoretical values of $\nabla^2\rho$ at the experimental position of the BCP, as this has been shown to improve the correspondence between experimental and theoretical topological properties.[24] However, in the case of **1** this brings about no significant improvement in the correspondence between theory and experiment.

It has also been suggested that in order to reproduce from theory the experimental topology of the polar C–O bonds, it is imperative to employ a high-level treatment of electron correlation and a large basis set.[25] However, this was not attempted in this study.

It has recently been pointed out that the multipolar model used to describe the experimental electron density to some extent introduces bias in the topological results.[26] The flexibility of the radial distribution has been identified as the main origin of the discrepancy.[27] Two methods have been suggested to diminish or determine the effect of such bias, both involve the use of a secondary theoretical electron density. This electron density is determined from a multipole refinement against theoretical 'noise-free' structure factors.

In one approach (the κ''-restricted multipole model or KRMM)[28] the radial κ''-parameters subsequently used in the refinement against experimental data are fixed on the values obtained from the refinement against the theoretical structure factors. The other method is simply a topological analysis of the theoretical electron density itself.

The topological analysis of the KRMM model gave, within the quoted esds, results similar to the ones given in Table 4, and was therefore omitted in the Table. Similarly, topological analysis of the secondary EDD resulted in very similar results, and since the level of theory used in the periodic DFT calculation was significantly lower than the single-point gas-phase calculation, the former results are not given.

Topology in non-bonded regions

The search for the experimental ring critical points (RCPs) revealed such in both ring B and C with values of ρ_{RCP} around 0.07(1) eÅ^{-3}, while the critical point in ring A was of a fundamentally different type, namely a cage critical point (CCP). In other words, along an axis perpendicular to the plane and through the geometrical center of ring A, the density reaches a local minimum exactly in this plane. The density in the CCP is 0.04(1) eÅ^{-3}. However, the positive curvature of the density perpendicular to the ring at the CCP is as high as 0.24e Å^{-5}, giving confidence to its significance. Directly above and below this CCP (distance ± 0.8 Å), on either side of ring A, two RCPs were found, exhibiting values of ρ_{RCP} around 0.05(1) eÅ^{-3}, however the Morse equation, which requires that a special relationship (#nuclei − #BCP + #RCP − #CCP = 0) remains fulfilled. This unexpected feature in the topology of **1** prompted us to investigate possible shortcomings in the modelling or, alternatively, find theoretical support for the observation.

Wavefunction analysis. To begin with the latter possibility, topological analysis of the single-point gas-phase wavefunction taken at the experimental geometry showed a clear RCP in the center of ring A. However, the crystal packing of **1** does exhibit π–π interactions between neighbouring molecules and the occurrence of the experimental CCP in ring A could be the result of these weak intermolecular interactions. Thus, we turned again to an analysis of the periodic wavefunction. Topological analysis of this wavefunction clearly retrieved a RCP in ring A (ρ_{RCP} = 0.13 eÅ^{-3}). Above and below this RCP, two CCPs are found with much smaller values of ρ (average ρ_{CCP} = 0.005 eÅ^{-3}). Hence, at this level of theory the experimental observation of a CCP in the centre of ring A cannot be reproduced.

Multipole refinement of theoretical structure factors. As mentioned above, the experimental electron density can be biased by the limited flexibility of the multipole model. Thus, the presence of a CCP in ring A in the electron density determined from the multipole refinement of theoretical structure factors would be a strong indication that the experimental observation of a CCP in ring A is an artefact from the multipole model employed. Interestingly, searching for the critical point in ring A revealed only a RCP with ρ_{RCP} = 0.11 eÅ^{-3}, very similar to the value found in the RCP's from the topological analysis of the periodic wavefunction. This lends far more credence to the experimental observation of a CCP in the center of ring A. However, it should be noted that the level of theory used for our periodic calculation is lower than those originally used by Volkov and Coppens to pinpoint the origin of bias from the multipole model on the experimental EDD (minimal basis set used was 6-21G).[27]

Fortunately, in addition to the presented dataset on **1**, one other high-resolution X-ray diffraction data sets on baicalein exists.[29] Topological analysis of the refined charge densities from this data set unambiguously shows a CCP in the center of ring A and two RCPs in close proximity above and below the CCP (ρ_{CCP} = 0.02(1) eÅ^{-3} and ρ_{RCP} = 0.04(1) eÅ^{-3}). This is the result irrespective of the complexity of the model used in the refinement, from the most crude model to a very sophisticated one.

We are therefore led to the conclusion that the observation of a CCP in the center of ring A is unlikely to be the result of systematic errors in the data. We have also shown that it is not an artefact of the multipolar model. However, if one takes into account the esds of the density at the critical points, one should only conclude that ρ is very flat along the "ring" axis in the experimental density. The electron density value at the CCP is not statistically different from that at the RCP since they differ by only one esd. Although there is some indication that the "true" topology could be different from that found theoretically (and the second experiment provides further support to this hypothesis), the only physical result from this experiment is that the electron density appears to be significantly more flat along the "ring" axis, than predicted theoretically. Whether this yields a different topology than found by theory, can not be safely concluded by the present analysis. Furthermore, as the CCP is not reproduced in high-level gas-phase calculations or less advanced periodic calculations, it might be viewed as a spurious feature. In part this may be explained by the following; based on the rigid bond test, we concluded that the thermal motion has been correctly deconvoluted from the EDD, small residual couplings may still remain. In the multipole refinement of theoretical structure factors, this coupling is implicitly set to zero. So, the occurrence of a different topology in the experiment could perhaps be the result of the small residual coupling, between thermal motion and EDD, in the multipole refinement of experimental structure factors. Perhaps another explanation could be the combined effects of three strongly electron-withdrawing substituents and π–π interactions, However, high-level single-point DFT(B3LYP, 6-31+G*) gas-phase calculations on a dimer of **1** did not give any CCP in ring A.

Hydrogen bonds and the charge distribution

Topological parameters of the HBs in **1** are given in Table 5. This table also features the local energy density values for the HBs calculated from Abramov's semi-empirical expression.[30]

Table 5 shows that for each HB type (oxygen or carbon donor), the bond strength descriptors (ρ_{BCP}, $\nabla^2\rho_{BCP}$, G_{BCP}, and $-V_{BCP}$) diminish as the HB-length (d_{1-2}) increases.

It is clear from Table 5 that the two O–H···O HBs at the top of Table 5 are significantly stronger than the other HBs

Table 5 Topological analysis of the hydrogen bonds in **1**

Bond$_{1-2}$	ρ_{bcp}/ eÅ^{-3}	$\nabla^2\rho_{bcp}$/ eÅ^{-5}	d_{1-2}/ Å	d_{1-bcp}/ Å	d_{2-BCP}/ Å	G_{bcp}	$-V_{bcp}$
H(4)—O(2)[a]	0.20(1)	4.68(1)	1.742	0.576	1.167	0.28	0.22
H(3)—O(2)	0.23(3)	2.64(6)	1.741	0.542	1.199	0.19	0.20
H(5)—O(4)[b]	0.10(1)	2.37(1)	2.004	0.743	1.261	0.13	0.09
H(11)—O(1)	0.08(1)	1.48(1)	2.378	1.031	1.347	0.08	0.06
H(9)—O(3)[c]	0.03(1)	0.42(1)	2.924	1.321	1.603	0.06	0.03
H(14)—O(5)[d]	0.04(1)	0.48(1)	3.029	1.385	1.645	0.03	0.02
H(14)—O(4)[d]	0.02(1)	0.25(1)	3.122	1.356	1.765	0.01	0.01
H(12)—O(2)[e]	0.02(1)	0.25(1)	3.233	1.537	1.696	0.01	0.01
H(11)—O(5)[f]	0.01(1)	0.18(1)	3.366	1.555	1.811	0.01	0.01
H(13)—O(2)[g]	0.01(1)	0.08(1)	3.485	1.490	1.995	0.03	0.02

[a] $+x, 3/2-y, 1/2+z$ [b] $1-x, 2-y, 2-z$ [c] $1-x, 1/2+y, 3/2-z$ [d] $x, y, -1+z$ [e] $2-x, 2-y, 1-z$ [f] $x, 5/2-y, -1/2+z$ [g] $2-x, 1/2+y, 1/2-z$.

in the Table. This is also evident from Fig. 5, which shows a pronounced polarisation of the oxygen lone pair (LP) on O(2) towards H(3). Such deformation is also recognised in the other short O–H···O HB (not shown). The extent of the polarisation of the LPs can be quantified by locating the LP positions and is performed by an automated search for maxima in $-\nabla^2\rho(r)$ using the program BUBBLE,[10] see Table 6.

The sum of the angles around O(2) is 350.3°, somewhat less than 360° expected for an sp^2-hybridised oxygen. This is due to the perturbation of LP2 towards H(4) out of the C(1)–O(2)···H(3) plane, showing the significant influence this HB has on the atomic electron density around O(2) and indirectly testifies that this HB is rather strong. The position of LP1 also shows the influence of hydrogen bonding on the EDD as the C(1)–O(2)–LP1 angle is decreased to 101.3° from the expected 120°, so as to almost completely match the C(1)–O(2)···H(3) angle of 100.7°.

It is worth examining the topology of the two shorter O–H···O HBs in a little more detail. Firstly, the value of $\nabla^2\rho_{BCP}$ in the first HB is about twice the value of $\nabla^2\rho_{BCP}$ in the second HB. This results from a larger positive curvature of ρ along the bond ($\lambda_3 = 6.9$ *vs* 6.0 eÅ^{-5}) and less negative curvatures perpendicular to the bond ($\lambda_1+\lambda_2 = -2.2$ *vs* -3.3 eÅ^{-5}). Furthermore, the second HB is the only HB with a negative total energy density ($H_{BCP} = G_{BCP} + V_{BCP}$), indicating that these bonds may be different in nature. Indeed, as seen in Fig. 1, the possibility for a resonance-assisted HB (RAHB) exists in the second HB, but not in any of the other HBs. The concept of RAHB was invoked by Gilli *et al.* to explain the presence of exceptionally short HBs in conjugated systems.[31] The existence of some degree of RAHB in the intramolecular O(3)–H(3)···O(2) HB may explain that this is slightly stronger than the other HB. In fact, in spite of similar donor–acceptor distances, it has a larger density value, a smaller parallel curvature and a slightly negative H_{BCP}.

The potential energy density (V_{BCP}) has been correlated to the HB energy (E_{HB}) by Espinosa *et al*,[32] using an empirical expression based on correlations between energy densities and H···O distances. Using this scheme, bond energies of 20 and 19 kcal mol^{-1} are derived for the two first HBs in Table 5, respectively, which, in the classification scheme for hydrogen bonds, characterises these bonds as strong.[33]

Table 6 Properties of the EDD at the O(2) lone pairs

	$\rho(r)$/ eÅ^{-3}	$\nabla^2\rho(r)$/ eÅ^{-5}	d(O–LP)/ Å	∠(C(1)–LP– H)/°
O(2)–LP1–H(3)	6.18	−121.6	0.345	168.5
O(2)–LP2–H(4)[a]	6.10	−111.7	0.346	163.8
∠LP1–O(2)–LP2 = 120.8°				

[a] $+x, 3/2-y, 1/2+x$.

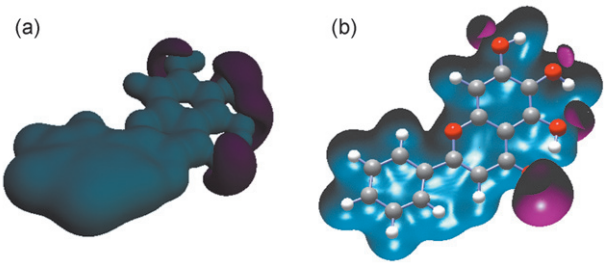

Fig. 6 (a) Experimental molecular electrostatic potential in **1**. The potential of +0.35 eÅ^{-1} is shown with the blue isosurface, the purple isosurface shows the −0.35 eÅ^{-1}-level. (b) Theoretical molecular electrostatic potential in **1**. Contours as in (a)

Crystal effects

One of the most intriguing results of the experimental charge density analysis are the quantitative measures of the intermolecular interactions. The intermolecular interaction energy can be calculated using the experimental charge density approach.[34] This leads to a lattice energy of −467(24) kJ mol^{-1} with a very large electrostatic contribution of −503(24) kJ mol^{-1}. The dispersion contribution from the π–π interaction between molecules is also significant at −247 kJ mol^{-1}.

The effect of the crystalline environment also has a pronounced influence on the molecular electrostatic potential (MEP), which is altered compared to the unperturbed gas-phase molecule, as found from a single-point theoretical calculation. This is shown in Figs. 6a and 6b, which represent the experimental and theoretical MEP, respectively.

Conclusion

Experimental evidence has been presented showing a (3,+3) cage critical point in the center of ring A in the flavone molecule, baicalein. This has been refuted by both gas-phase and periodic calculations on the same molecule. However, systematic errors in experimental data and bias from the multipole model have been ruled out as plausible explanations for this discrepancy. Thus, we suggest that the combination of strongly electron-withdrawing substituents on the phenyl-ring and the dispersive character of its weak intermolecular π–π-interactions may not be adequately described at the level of theory, which may cause the discrepancy in the electron density. We intend to continue our studies of flavone compounds and will address the topology of the electron density in the relevant ring A in future work.

The experimental electron density approach also shows the large potential for such studies to quantify a wide range of hydrogen bond motifs. In particular, deviations from structural predictions are found in this study, which show that the parameters that influence hydrogen bond strength are still not completely understood.

Acknowledgements

The authors thank the Australian Research Council for funding this work and the Australian Centre for Advanced Computing and Communications (ac3) [http://www.ac3.com.au] for a generous allocation of computer resources. We would also like to thank Dr Hong Jie Wang for supplying a sample of Baicalein. One author (JO) thanks the Danish Natural Science Research Council for financial support.

References

1 S. Chen, Q. Ruan, E. Bedner, A. Deptala, X. Wang, T. C. Hsieh, F. Traganos and Z. Darzynkiewicz, *Cell Prolif.*, 2001, **34**, 293–304.
2 B. Q. Li, T. Fu, Y. Dongyan, J. A. Mikovits, F. W. Ruscetti and J. M. Wang, *Biochem. Biophys. Res. Commun.*, 2000, **276**, 534–538.
3 Z.-H. Shao, T. L. Vanden Hoek, Y. Qin, L. B. Becker, P. T. Schumacker, C-Q. Li, L. Dey, E. Barth, H. Halpern, G. M. Rosen and C.-S. Yuan, *Am. J. Physiol., Heart and Circulatory Physiology*, 2002, **282**, H999–H1006.
4 T. Hong, G.-B. Jin, S. Cho and J.-C. Cyong, *Planta Medica*, 2002, **68**, 268–271.
5 I. Startchik, D. Morabito, U. Lang and M. F. Rossier, *J. Biol. Chem.*, 2002, **277**, 24 265–24 273.
6 T. Nishioka, J. Kawabata and Y. Aoyama, *J. Nat. Prod.*, 1998, **61**, 1413–1415.
7 J. Ai, K. Dekermendjian, X. Wang, M. Nielsen and M.-R. Witt, *Drug Dev. Res.*, 1997, **41**, 9–106.
8 M. J. Frisch, G. W. Trucks, H. B. Schlegel, G. E. Scuseria, M. A. Robb, J. R. Cheeseman, V. G. Zakrzewski, J. A. Montgomery Jr., R. E. Stratmann, J. C. Burant, S. Dapprich, J. M. Millam, A. D. Daniels, K. N. Kudin, M. C. Strain, O. Farkas, J. Tomasi, V. Barone, M. Cossi, R. Cammi, B. Mennucci, C. Pomelli, C. Adamo, S. Clifford, J. Ochterski, G. A. Petersson, P. Y. Ayala, Q. Cui, K. Morokuma, D. K. Malick, A. D. Rabuck, K. Raghavachari, J. B. Foresman, J. Cioslowski, J. V. Ortiz, A. G. Baboul, B. B. Stefanov, G. Liu, A. Liashenko, P. Piskorz, I. Komaromi, R. Gomperts, R. L. Martin, D. J. Fox, T. Keith, M. A. Al-Laham, C. Y. Peng, A. Nanayakkara, C. Gonzalez, M. Challacombe, P. M. W. Gill, B. Johnson, W. Chen, M. W. Wong, J. L. Andres, C. Gonzalez, M. Head-Gordon, E. S. Replogle and J. A. Pople, *Gaussian 98, Revision A. 7*, Gaussian, Inc., Pittsburgh PA, 1998.
9 (*a*) A. D Becke, *J. Chem. Phys.*, 1993, **98**, 5648; (*b*) C. Lee, W. Yang and R. G. Parr, *Phys. Rev. B*, 1988, **38**, 3098; (*c*) P. J. Stevens, F. J. Devlin, C. F. Chabalowski and M. J. Frisch, *J. Phys. Chem.*, 1994, **98**, 11 623; (*d*) C. Adamo and V. Barone, *Chem. Phys. Lett.*, 1997, **274**, 242.
10 R. F. W. Bader, *Atoms in Molecules a Quantum Theory*, Clarendon Press, Oxford, 1990.
11 V. R. Saunders, R. Dovesi, C. Roetti, M. Causà, N. M. Harrison, R. Orlando and C. M. Zicovich-Wilson, CRYSTAL98 Users Manual, University of Torino, Italy, 1998.
12 C. Gatti, TOPOND98 Users Manual, CNR-ISTM, Milano, Italy, 1999.
13 SAINT+: Area-Detector Integration Software., Siemens Industrial Automation, Inc., Madison, WI, 1995.
14 R. H. Blesssing, *J. Appl. Crystallogr.*, 1989, **22**, 396.
15 G. M. Sheldrick, *SHELXL-97, Program for refinement of crystal structures*, University of Göttingen, Germany, 1997.
16 F. H. Allen, O. Kennard, D. G. Watson, L. Brammer, A. G. Orpen and R. J. Taylor, *J. Chem. Soc., Perkin Trans. 2*, 1987, S1–S9.
17 T. Koritsanszky, S. T. Howard, P. R. Mallinson, Z. Su, T. Richter and N. K. Hansen, XD—a computer program package for the multipole refinement and analysis of electron densities from diffraction data. Free University of Berlin, 1997.
18 N. K. Hansen and P. Coppens, *Acta Crystallogr. Sect. A*, 1979, **39**, 909–921.
19 P. Coppens, X-ray Charge Densities and Chemical Bonding, Oxford Press, 1997.
20 F. L. Hirshfeld, *Acta Crystallogr. Sect. A*, 1976, **32**, 239–244.
21 B. J. Hall, J. R. Hanrahan, G. A. R. Johnston, T. W. Hambley and D. E. Hibbs, *Acta Crystallogr. Sect. E*, 2001, **57**, o592–o593 and references therein.
22 Perhaps the earliest observation of a closed-shell C–O bond interaction is presented in the benchmark study of citrinin. P. Roversi, M. Barzaghi, F. Merati and R. Destro, *Can. J. Chem.*, 1996, **74**, 1145–1161.
23 A similar result was obtained in the charge density study of taurine. D. E. Hibbs, C. A. Austin-Woods, J. A. Platts, J. Overgaard and P. Turner, *Chem. Eur. J.*, 2003, **9**, 1075–1084.
24 C. Gatti, R. Bianchi, R. Destro and F. Merati, *J. Mol. Struct. Theochem*, 1992, **87**, 409–433.
25 H. Birkedal, PhD Thesis, University of Lausanne, Switzerland, 2000.
26 S. T. Howard, M. B. Hursthouse, C. W. Lehmann and E. A. Poyner, *Acta Crystallogr. Sect. B*, 1995, **51**, 328–337.
27 A. Volkov and P. Coppens, *Acta Crystallogr. Sect. A*, 2001, **57**, 395–405.
28 Yu. A. Abramov, A. Volkov and P. Coppens, *Chem. Phys. Lett.*, 1999, **311**, 81–86.
29 The additional dataset (from a different crystal) was refined with the same procedure as described for this dataset. Final $R(F^2)$ values was 0.058, thus not of entirely the same quality as the one presented. However, the data are the result of a careful diffraction experiment performed at 100 K using the same experimental facility.
30 Yu. A. Abramov, *Acta Crystallogr. Sect. A*, 1997, **53**, 264–272.
31 G. Gilli, F. Bellucci, V. Ferretti and V. Bertolasi, *J. Am. Chem. Soc.*, 1989, **111**, 1023–1028.
32 E. Espinosa, E. Molins and C. Lecomte, *Chem. Phys. Lett.*, 1998, **285**, 170–173.
33 F. Hibbert and J. Emsley, *Adv. Phys. Org. Chem.*, 1990, **26**, 255–379.
34 Yu. A. Abramov, A. Volkov, G. Wu and P. Coppens, *Acta Crystallogr. Sect. A*, 2000, **56**, 585–591.